Contrib Mineral Petrol (2007) 153:689–698
DOI 10.1007/s00410-006-0170-8

ORIGINAL PAPER

Thermochemistry and melting properties of basalt

**M. A. Bouhifd · P. Besson · P. Courtial ·
C. Gérardin · A. Navrotsky · P. Richet**

Received: 22 June 2006 / Accepted: 1 December 2006 / Published online: 29 December 2006
© Springer-Verlag 2006

Abstract The heat capacities of the liquid, glassy and crystalline phases of an alkali basalt have been determined from relative enthalpies measured between 400 and 1,800 K. Values given by available models of calculation generally agree to within 2% of these results. As derived from the new data and the enthalpy of vitrification measured at 973 K by oxide-melt drop solution calorimetry for the same sample, the enthalpy of fusion of this basalt increases from 15.4 kJ/mol at 1,000 K to 33.6 kJ/mol at 1,800 K. Comparisons between the enthalpies of fusion of basalt and model compositions confirm the small magnitude of the enthalpy of mixing between the molten mineral components of the liquids. Minor variations in the chemical composition have only a small effect in the heat capacity and the enthalpy of melting of basalt. The enthalpies of formation at 298 K from the oxides of the crystallized and glass phases of this alkali basalt are –112.2 and –98.5 kJ/mol, respectively, for a gram formula weight based on one mole of oxide components.

Introduction

As a result of the age of the earth controversy triggered by Kelvin (see Burchfield 1990), it was early recognized that quantitative understanding of melting of basalt at room and high pressure was a key ingredient for deciphering the early history of our planet. This dispute eventually resulted in measurements by Barus (1893) made in the USA at the request of King (see King 1893), which yielded an enthalpy of fusion of about 100 J/g for basalt at 1,200°C and 67 J/g at 1,100°C. At the same time, similar determinations of melting properties undertaken in Britain by Roberts-Austen and Rücker (1891) revealed the thermochemical complications arising from glass formation when basalt liquids are rapidly cooled.

Barus' result was deemed to be too low because of basalt vitrification. Therefore, a value of 418 J/g was suggested by Bowen (1913) for the enthalpy of melting of basaltic magma as obtained from estimated enthalpies of fusion of common rock-forming minerals such as diopside. Although basalts and basaltic melts have a

Communicated by J. Hoefs.

M. A. Bouhifd · P. Richet
Physique des Minéraux et des Magmas, IPGP,
4 Place Jussieu, 75252 Paris Cedex 05, France

M. A. Bouhifd (✉)
Department of Earth Sciences, Oxford University,
Parks Road, OX1 3PR Oxford, UK
e-mail: alib@earth.ox.ac.uk

P. Besson
Equipe de Volcanologie, IPGP, CNRS UMR 7164,
4 Place Jussieu, 75252 Paris Cedex 05, France

P. Courtial
Department of Earth and Environmental Sciences,
Munich University, Theresienstr. 41/III,
80333 Munich, Germany

C. Gérardin · A. Navrotsky
Thermochemical Facility, NEAT ORU,
University of California at Davis,
Davis, CA 95616-8779, USA

Present Address:
C. Gérardin
UMR 5618 ENSCM-UM1-CNRS,
ENSCM Montpellier, France

considerable petrologic importance on their own, these pioneering studies have regrettably long remained unfollowed. Only in the 1970s these early data have been complemented by the drop calorimetry observations of Lindroth and Krawza (1971) and Bacon (1977) on crystalline and glassy basalt samples, whereas attempts were then made at estimating the enthalpy of fusion of basalt from yet uncertain melting data for forsterite, diopside and anorthite (i.e., Yoder 1976).

More recently, enthalpies of fusion have been determined for a number of silicate minerals (e.g., Weill et al. 1980; Stebbins et al. 1983, 1984; Richet and Bottinga 1984a, 1986; Ziegler and Navrotsky 1986; Lange et al. 1991; Richet et al. 1993a). Such determinations have also been performed for binary or ternary systems (Navrotsky et al. 1989; Tarina et al. 1994; Kojitani and Akaogi 1997; Sugawara and Akaogi 2003), and for basalt or model basalt compositions (Fukuyama 1985; Lange et al. 1994; DeYoreo et al. 1995; Kojitani and Akaogi 1995; Tsuruta and Takahashi 1998). These data are crucial to setup thermodynamic models of chemical mass transfer in magmatic systems such as MELTS (Ghiorso and Sack 1995) and the models developed by Holland and Powell (1998) or Asimow et al. (2001).

In this study we have made a comprehensive thermochemical study of an alkali basalt to complement these measurements and to allow more accurate thermodynamic treatment of partial melting and crystallization. From drop-calorimetry experiments, we have first determined the heat capacity of the crystalline, liquid and glassy phases. Together with oxide-melt solution calorimetry measurements of the enthalpy of vitrification, these data then make it possible to determine accurately the enthalpy of melting over wide temperature intervals. Because these measurements extend the investigated composition range of basalts, we finally review available data in the light of the influence of composition on heat capacity and enthalpy of fusion and confirm that enthalpies of mixing in basalt systems are small when taking mineral compositions as components.

Experimental methods

Basalt sample

An alkali natural basalt from Stein-Frentz, Germany, (hereafter called SFB) previously investigated in a viscometry and cristallization study (Bouhifd et al. 2004) was chosen as a starting material. The basalt was first melted at 1,770 K in air and quenched as a glass. The chemical composition of this glass as obtained from electron microprobe analyses is compared in Table 1 with those of basalts investigated in previous calorimetric studies. Included in Table 1 are the formula weight of the SFB sample for a total of one mole of oxide components; the numbers of atoms per formula weight, which constitutes a useful framework for comparing the thermodynamic properties of related liquids; and the room-temperature density of the SFB glass measured with an Archimedean method (toluene used as immersion liquid). We also listed the redox ratio as determined by wet chemical analyses for SFB glass (Bouhifd et al., 2004). Along with the total Fe analyzed, this analysis yields Fe_2O_3 and FeO concentrations of 5.4 and 6.4 wt%, respectively. These concentrations are in relatively good agreement with the calculated values using the model of Kress and Carmichael (1988) which includes natural liquid data equilibrated in air (Kilnic et al. 1983) (with our basalt composition quenched to a glass from 1,770 K).

The liquidus temperature of the Stein-Frentz basalt was determined from optical microscopy observations of charges quenched after annealing in air in a gradient furnace. Spinel was the first liquidus phase, crystallizing at 1,570 ± 10 K in heating experiments made from room temperature and disappearing at the same temperature in cooling experiments made from 1,700 K. To obtain a completely crystalline sample for the

Table 1 Chemical composition (wt%) of the materials investigated in this work and in previous studies

	SFB	Dresser Basalt[a]	Olivine Basalt[b]
SiO_2	46.58	48.42	48.83
Al_2O_3	13.28	15.23	12.04
Na_2O	5.60	2.30	2.42
K_2O	1.38	0.58	1.93
FeO	6.38	6.70	2.51
Fe_2O_3	5.35	6.60	5.77
CaO	10.00	8.35	7.36
MgO	9.15	6.14	16.69
MnO	0.19	0.18	0.18
TiO_2	2.45	1.90	1.19
P_2O_5			0.54
		2.26[c]	
Total	100.36	98.66	99.46
ρ (g/cm^3)[d]	2.862		
$Fe^{2+}/\sum Fe$[e]	0.43		

Average of 10 analyses made with a Camebax electron microprobe

[a] Lindroth and Krawza (1971)

[b] Lange et al. (1994)

[c] Loss on ignition at 1273 K

[d] Room temperature Archimedean density of the glass

[e] $Fe^{2+}/\sum Fe$ determined by wet chemical analyses

calorimetric measurements, the glass was heated overnight near 1,400 K.

Mineral composition

As the grain size of the mineral grains in our crystalline samples ranged from 50 to 150 nm (see Bouhifd et al. 2004), we have analyzed by analytical electron microscopy a total of 400 mineral grains for four different preparations to determine the actual mineralogical composition of the crystallized SFB. The samples were examined by Analytical Transmission Electron Microscopy (ATEM) with a JEOL 2000 EX TEM/STEM microscope operated at 200 kV and 15 μA. The TEM observations were made directly on a fine powder deposited on a carbon film mesh. The mineral phases comprising the particles were identified by X-ray microanalyses performed with a Si(Li) energy-dispersive system (EDS) over a zone of about 100 nm. Because of the presence of a beryllium window protecting the Si(Li) crystal, analysis of elements lighter than magnesium, including oxygen, was impossible. Selected area electron diffraction (SAED) patterns also allowed us to identify the different crystals. The average chemical compositions of the observed olivine, clinopyroxene, plagioclase, feldspars and spinel are reported in Table 2. Assuming the counts to be proportional to the volume fractions of minerals, we calculated the modal composition given below. In modeling studies, this composition is often assumed to be close to the composition $Di_{49.0}An_{43.5}Fo_{7.5}$ (wt%) in the diopside–anorthite–forsterite system (cf. Osborn and Tait 1952; Yoder 1976; Kojitani and Akaogi 1995). To take into account sodium oxide, a plagioclase component can be added, giving an approximate $Di_{28.5}An_{33.5}Fo_{4.5}Ab_{33.5}$ (wt%) formula (Yoder and Tilley 1962). In the following, and for our thermodynamic calculations and comparisons with the experimental data, we approximate the mineralogical composition of SFB basalt to 28 wt% $An_{60}Ab_{40}$, 12 wt% $Or_{60}Ab_{40}$, 7 wt% $Fo_{70}Fa_{30}$, 43 wt% $Di_{60}Wo_{40}$ and 10 wt% $Hem_{80}Ilm_{20}$, where An is anorthite $CaAl_2Si_2O_8$, Ab is albite $NaAlSi_3O_8$, Or is orthoclase $KAlSi_3O_8$, Fo is forsterite Mg_2SiO_4, Fa is fayalite Fe_2SiO_4, Di is diopside $CaMgSi_2O_6$, Wo is wollastonite $CaSiO_3$, Hem is hematite Fe_2O_3 and Ilm is ilmenite $FeTiO_3$.

Table 2 Average chemical compositions (wt%) and volume fractions of mineral phases in crystallized SFB

	Plagioclase	Alkali-feldspar	Clinopyroxene	Olivine	Spinel
SiO_2	51.8	65.9	59.1	41.3	
Al_2O_3	29.8	19.3	6.5	0.7	14.3
Na_2O	4.7	4.3	0.7	0.7	
K_2O	0.2	10.0	0.3	0.1	
FeO	0.4	0.1	9.3	22.2	68.2
CaO	13.0	0.4	15.2	0.8	
MgO			6.3	34.1	9.4
TiO_2	0.1	0.1	2.7	0.2	8.0
Volume %	33	25	23	14	5

Average of more than 20 chemical analyses made by Analytical Transmission Electron Microscopy. Total iron expressed as FeO

Drop calorimetry

Heat capacities were determined from relative-enthalpy measurements H_T–$H_{273.15}$ (hereafter denoted H_{273}) made with the drop method in an ice calorimeter. Working between 900 and 1,800 K, and 400 and 1,100 K, respectively, the two different calorimetric setups used have already been described in detail (Richet et al. 1982, 1992). Experiments on sapphire indicate that the imprecision and inaccuracy of the measured enthalpies are less than 0.05 and 0.2%, respectively, whereas the instrumental inaccuracy of the derived heat capacities is less than 0.5%. By taking into account uncertainties in the chemical compositions, errors of less than 1% are estimated for the reported molar heat capacities.

About 5 g of material were run in Pt–Rh 15% crucibles, the two 1.5 mm openings of which were tightly closed with crimped platinum foil, leaving less than 0.5 cm^3 of air in contact with the samples. To limit possible changes in the iron redox ratio of the sample, the crucible was heated in an argon atmosphere, and the heating period was kept as short as possible. In all cases, the sample was heated for less than 45 min above 1,000 K. After the drop, cooling of the crucible down to 273.15 K took about 20–30 min. No significant weight variations of the material due to redox changes were observed. In addition, the measured enthalpies show no anomalous high scatter, which also indicates that the effects of possible changes in the oxidation state of iron were within the uncertainties of calorimetric measurements.

Solution calorimetry

The enthalpies of solution of samples in lead borate were measured in a high-temperature Calvet twin microcalorimeter as described in detail by Navrotsky (1997). In brief, samples of about 50 mg were dropped from room temperature in the oxide melt at 973 K. The difference in enthalpy of solution of reactants and products thus yields the enthalpy of the reaction at room temperature (Navrotsky 1997).

Heat capacity and relative enthalpy

General remarks

The relative enthalpies are listed in Table 3 where runs are labeled in chronological order for each series of experiments. Measurements made with the lower-temperature setup are indicated by the suffix B. The results are plotted in Figs. 1 and 3 in the form of mean heat capacities

$$C_m = (H_T - H_{273})/(T - 273). \qquad (1)$$

The slight temperature dependence of C_m allows the calorimetric data to be plotted at an expanded scale, without the fitting bias that can beset the derived heat capacities. These heat capacities were determined from least-squares fits made to the experimental enthalpies with

$$C_p = (\partial(H_T - H_{To})/\partial T)_p. \qquad (2)$$

As usual, the calorimetric data could be reproduced within their error margins with Maier–Kelley equations,

$$C_p = a + bT + c/T^2 + d/T^{0.5}. \qquad (3)$$

Table 3 Relative enthalpies of the materials investigated (J/g)

No.	$T(K)$	H_T–H_{273}	No.	T(K)	H_T–H_{273}
Crystalline SFB			SFB glass and liquid		
FF.14	475.2	171.60	EI.1-B	430.4	131.44
FF.16	684.4	381.36	EI.2-B	494.7	192.69
FF.5	700.5	399.23	EI.3-B	594.5	292.22
FF.4	798.4	504.38	EI.4-B	689.9	392.38
FF.6	862.3	574.17	EI.5-B	718.4	424.14
FF.8	1070.4	812.35	EI.6-B	767.0	475.91
			EI.7-B	819.8	534.33
FH.6	526.8	221.16	EI.18-B	851.6	569.40
FH.4	613.5	307.56	EI.8-B	911.0	637.21
FH.7	727.6	428.19	EI.9-B	962.7	695.97
FH.2	910.5	628.44	EI.11-B	976.4	717.35
FH.8	960.0	685.29	EI.21	986.2	730.31
FH.9	1161.1	915.24	EI.19	1049.9	822.82
			EI.14	1105.8	910.27
			EI.15	1139.6	963.
			EI.16	1202.2	1039.28[a]
			EI.17	1658.9	1754.02
			EI.20	1700.3	1818.29

[a] Partial crystallization of the sample in the furnace before the drop

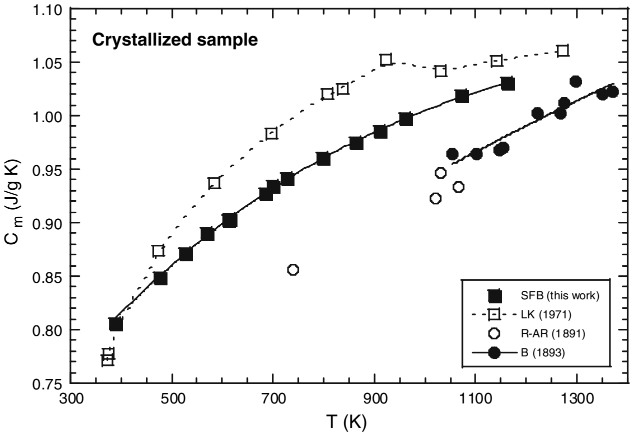

Fig. 1 Mean heat capacities reported for crystallized basalts: *LK* Lindroth and Krawza (1971); *R-AR* Roberts-Austen and Rücker (1891); *B* Barus (1893). The *dashed line* represents the fitted values as given by the enthalpy equation of Table 3. The H_T–H_{300} data of Lindroth and Krawza (1971) have been converted to H_T–H_{273} with the C_p model of Berman and Brown (1985)

Crystallized basalt

Experiments were made up to about 1,200 K, i.e., below the liquidus temperature of 1,430 K determined in preliminary experiments made by differential thermal analysis. The results are compared in Fig. 1 with previously published data. On a Joule/gram basis, our results are intermediate between the early enthalpies of Roberts-Austen and Rücker (1891) and those of Barus (1893) and the more recent observations of Lindroth and Krawza (1971). The difference with the latter is about 8% and is unlikely due only to differences in chemical composition. As to the abrupt change observed near 850 K in the data of Lindroth and Krawza (1971), it is probably due to the effects of the ferro- to paramagnetic transition of magnetite which constituted about 5 vol% of the basalt investigated by these authors.

The C_p coefficients and relative enthalpy equations are given in Table 4 and reported in Fig. 2. These results can be compared with model values predicted from either mineral or oxide components. With mineral components, the heat capacity of basalt is obtained directly from a summation of the mineral C_p's:

$$C_{pm} = \sum x_i C_{pmi}, \qquad (4)$$

where x_i and C_{pmi} are the mole fraction and the heat capacity of mineral i, respectively. As shown in Fig. 2, agreement to within 2% is obtained for SFB from the values compiled by Robie and Hemingway (1995) for fayalite, albite, orthoclase and ilmenite, from those

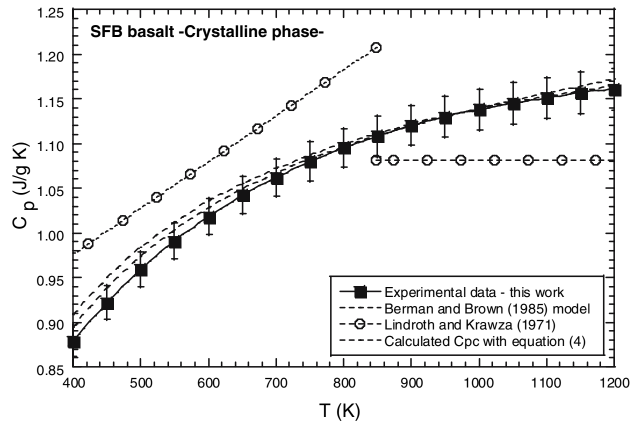

Fig. 2 Heat capacity of crystallized SFB: experimental values of this work and of Lindroth and Krawza (1971), values calculated with model of Berman and Brown (1985) (BB) and derived from Eq. (4) with our model of mineralogical composition of basalt

determined by Richet and Fiquet (1991) for anorthite and diopside, and by Gillet et al. (1991) for forsterite. The heat capacities calculated for our basalt with Eq. (4) from the observed mineralogical composition are similar and are within the uncertainties of the experiments. It follows that the mineralogical changes induced by minor differences in chemical composition have small effects on the heat capacity and relative enthalpy of basalt.

In terms of oxide components the heat capacity of basalt is alternatively given by:

$$C_{pm} = \sum x_i \bar{C}_{pi} \tag{5}$$

where x_i is the mole fraction of oxide i in the mineral considered. The data derived in this way from the model of Berman and Brown (1985) also reproduce the measured values to within approximately 2% (Fig. 2). Of course, the success of such an additive model lies in the low sensitivity of the high-temperature C_p of crystals to structural factors.

Basalt glass and liquid

The experimental relative-enthalpy values for glassy and liquid phases are reported in Table 3 and plotted in Fig. 3a. In Fig. 3b we have also plotted the experimental values in the form of mean heat capacities because this representation provides a plot of the raw data at an expanded scale, without any fitting bias that can beset the derived heat capacities. In this plot the glass transition shows itself as a sharp break in the slope of the mean heat capacity curve. The glass transition of our basalt, T_g = 960 K, is given by the intersection of the enthalpy equations of the glass and liquid phases of the material. In addition, partial crystallization of the sample in the furnace before the drop is revealed by the anomalously low result of the experiment performed at 1,202 K for the supercooled liquid.

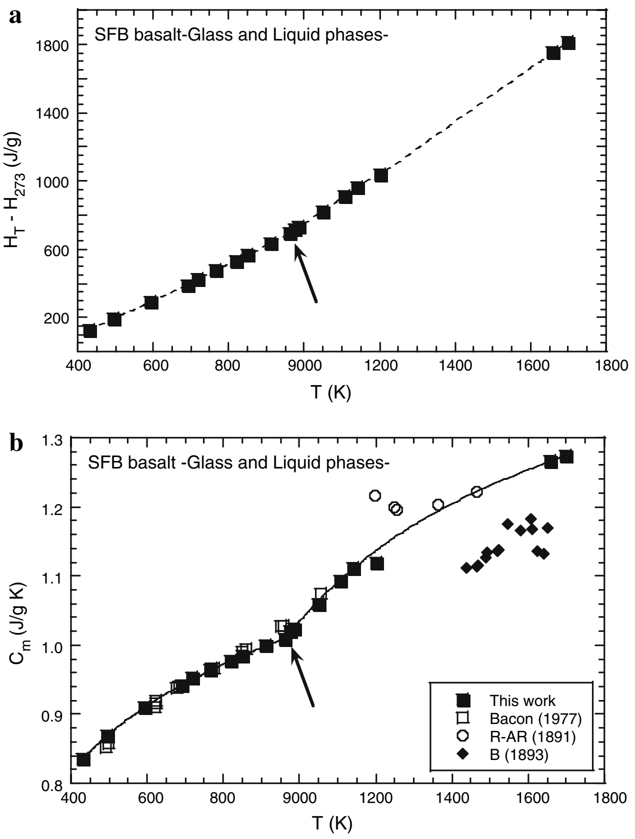

Fig. 3 **a** Relative enthalpy, H_T–H_{273}, for glassy and molten SFB basalt. The *arrow* indicates the glass transition temperature. **b** Mean heat capacities reported for glassy and molten basalts: Bacon (1977); *R-AR* Roberts-Austen and Rücker (1891); *B* Barus (1893). The *arrow* indicates the glass transition, the *solid lines* the fitted values as given by the enthalpy equations of Table 3. The H_T–H_{300} data of Bacon (1977) have been converted to H_T–H_{273} with the C_p model of Richet (1987)

Once more, we point out that the glass transition takes place when the glass C_p becomes close to the harmonic limit of the isochoric heat capacity (C_v), namely 3R per gram atom (= 25.0 J/g atom K) where R is the gas constant (see Richet and Bottinga 1986). Below the glass transition, the H_T–H_{300} data of Bacon (1977) agree with the new results within the combined errors of the measurements (Fig. 3b). This indicates that minor composition differences, such as variations in ferrous–ferric ratios, do not have significant effects on the heat capacity of basalt glass. The glass transition temperatures are also similar in both studies, consistent with the fact that the cooling rates were similar. In the supercooled liquid region, the single measurement

Table 4 Coefficients of $C_p = a + bT + c/T^2 + d/T^{0.5}$ (J/g K) and $H_T – H_{273} = R_{273} + \int C_p \, dT$ (J/g)[a]

	a	$10^3\ b$	$10^{-5}\ c$	$10^{-2}\ d$	R_{273}	ΔT (K)	AAD (%)
Glass	0.9576	0.2321	–0.2397	0.		430–910	0.07
Liquid[a]	1.4426	0.0594	0.	0.	–720.49	963–1,700	0.08
Solid	2.3370	–0.2773	0.2202	–0.2976		475–1,160	0.09

ΔT is the temperature interval investigated and AAD the average absolute deviation of the fitted enthalpies from the experimental values

[a] AAD of 0.13% with a constant C_p of 1.522 J/g

made by Bacon (1977) at 1,055 K also agrees with our results, whereas the experimental data of Barus (1893) are systematically lower than ours. This might be due to partial crystallization of the supercooled liquid during the heating stage of their measurements (Fig. 3b).

As shown in Fig. 4a, the values predicted by the model of Richet (1987) for glasses are within 1% of the values given in Table 3. As to the similarities between the relative enthalpies of the crystalline and glassy phases (Fig. 5), they simply reflect the aforementioned insensitivity of the high-temperature heat capacity of solids to structural factors (e.g., Robinson and Haas 1983; Richet et al. 1993b).

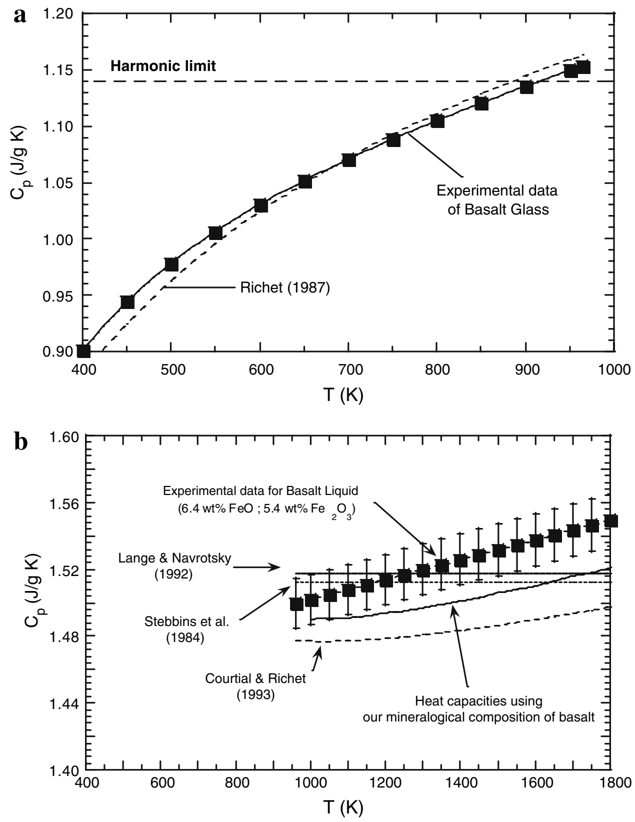

Fig. 4 **a** Measured capacities of glassy SFB basalt and values calculated with the model of Richet (1987). **b** Measured heat capacities of liquid SFB basalt (the reported errors are ±1%) and values calculated with the models of Stebbins et al. (1984), Lange and Navrotsky (1992), Courtial and Richet (1993) and the heat capacities using our mineralogical composition of basalt

For molten SFB, a fit made with a constant C_p yields a value of 1.522 J/g K which agrees to within 0.7 and 0.3% with the empirical model values of Stebbins et al. (1984) and Lange and Navrotsky (1992), respectively. Such comparisons refer to average values over wide temperature intervals; however, because our enthalpy data are reproduced within their experimental errors only with a temperature-dependent heat capacity (Table 4) as previously observed in extensive high-precision measurements made on a variety of aluminosilicate melts (Richet and Bottinga 1985; Courtial and Richet 1993; Bouhifd et al. 1998).

In contrast to the heat capacities of the glass phase, this temperature-dependent C_p is not very well reproduced, especially at high temperatures, with available models of calculations based on oxide components (Stebbins et al. 1984; Lange and Navrotsky 1992; Richet and Bottinga 1985; Courtial and Richet 1993). The differences being the lowest for the models of Stebbins et al. (1984), and Lange and Navrotsky (1992) at lower temperatures (Fig. 4b). This is further evidence for the complex behavior of aluminosilicate liquids with respect to heat capacity. One can alter-

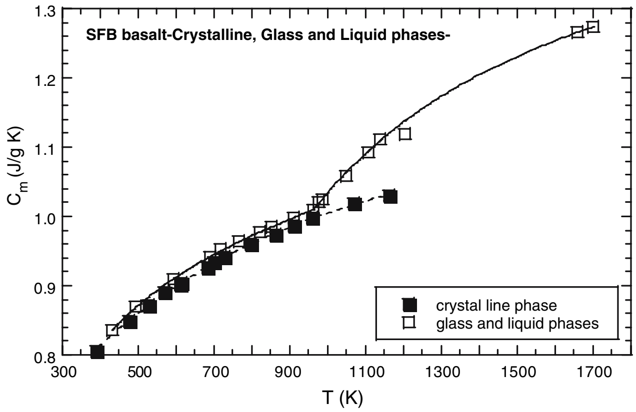

Fig. 5 Comparison between the mean heat capacities of the crystal and glass phases of SFB basalt

natively select molten minerals as melt components. The results obtained with such available data (Richet and Bottinga 1984a, b) and calculated values for $FeTiO_3$, Mg_2SiO_4 and Fe_2SiO_4 (Richet and Bottinga 1985) are shown in Fig. 4b. These results reproduce the temperature-dependent C_p within 2%, and they underline the importance of binary interactions between aluminum and alkaline or alkaline earth cations, which are thus simply taken into account when such complex components are selected.

Enthalpy of melting

The enthalpy of fusion (ΔH_f) of a crystalline material can be determined at any temperature T from the enthalpy difference ΔH_{g-c} between the crystalline and the liquid (or glass) phases at a given temperature T_v and the heat capacities of the relevant phases. If T_v is lower than the glass transition temperature (T_g), one has then

$$\Delta H_f = \Delta H_{g-c}(T_v) + \int_{T_v}^{T_g} (c_{pg} - c_{pc})\mathrm{d}T + \int_{T_g}^{T_f} (c_{pl} - c_{pc})\mathrm{d}T, \tag{6}$$

where C_{pg}, C_{pl} and C_{pc} are the heat capacities of the glass, liquid and crystalline phases, respectively. In this study, our T_v of 973 K was slightly higher than the drop-calorimetry glass transition temperature (T_g = 960 K). Hence, we actually measured the enthalpy difference between the supercooled liquid and the crystalline material, viz

$$\Delta H_f = \Delta H_{l-c}(T_v) + \int_{T_v}^{T_f} (c_{pl} - c_{pc})\mathrm{d}T. \tag{7}$$

The ΔH_{l-c} data at T_v are listed in Table 5 along with the standard deviation and the errors (%) of the measurements.

Table 5 Drop-solution experiments at 973 K on SFB and derived enthalpy of vitrification (J/g)

	Liquid	Crystalline
	720	959
	717	962
	717	948
	720	943
	720	950
Mean ΔH	718.8	952.4
σ	±1.6	±7.9
Error (%)	0.2	0.8
ΔH_{l-c}	233.6 ± 2.5	

For basalt, integration of Eq. (9) with the heat capacities of the glass, liquid and crystalline phases and the ΔH_{l-c} data at T_v yields for the enthalpy of fusion (J/g) over wide temperature intervals in the following equation:

$$\Delta H_f(T) = -984.226 - 0.8147\,T + 0.1387 \times 10^{-3}\,T^2 + 0.2202 \times 10^5 1/T + 0.5952 \times 10^2\,T^{0.5}, \tag{8}$$

where temperatures are in Kelvin and enthalpies in Joule/gram. As shown in Fig. 6, the variation of ΔH_f (T) given by Eq. (10) is almost linear at temperatures higher than 973 K. Hence, the enthalpy of fusion of basalt can be derived more simply from the linear fit made to the values yielded by Eq. (10), namely:

$$\Delta H_f(T) = -118.48 + 0.36311\,T(\mathrm{K}). \tag{9}$$

With these equations we derive an enthalpy of fusion of ΔH_f = 400.8 J/g for SFB at 1,430 K ($\Delta H_f \approx$ 25.6 kJ/mol). This value is in good agreement with the early datum of Bowen (1913). Before comparing our result with recently published enthalpies of fusion for basalts, we must note that these data are in fact the summation of ΔH_f of endmember minerals in the forsterite–diopside–anorthite system (Yoder 1976; Fukuyama 1985; Kojitani and Akaogi 1995). Fukuyama (1985) reported that enthalpies of fusion for eutectic liquids in the system anorthite–diopside and forsterite–diopside–anorthite, for haplobasaltic liquid in equilibrium with olivine and two pyroxenes in the system forsterite–diopside–SiO_2 and for basaltic melts from natural peridotite parent, are about 546, 506, 656 and 675 J/g, respectively. Kojitani and Akaogi (1995) gave an enthalpy of fusion of basalt of the order of 506 J/g at 1,543 K, for a eutectic composition in the system diopside–anorthite–forsterite (Di:Fo:An = 49.0:7.5:43.5 wt%). One can also note that

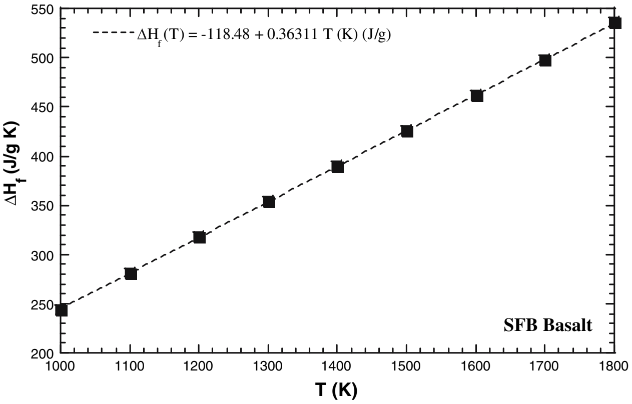

Fig. 6 Enthalpy of melting of SFB basalt as a function of temperature

direct measurements for the enthalpy of fusion of basalt were made by Lange et al. (1994) and Kojitani and Akaogi (1995) and gave similar results.

To compare our results at the same temperature we have used the following equation:

$$\Delta H_{\mathrm{f}}(T_1) = \Delta H_{\mathrm{f}}(T_2) - \int_{T_1}^{T_2} (c_{\mathrm{pl}} - c_{\mathrm{pc}})\mathrm{d}T, \qquad (10)$$

where C_{pl} and C_{pc} are the coefficients of the heat capacities of liquid and crystalline basalt, respectively, determined in this work.

These comparisons suggest that the enthalpy of mixing between the molten mineral components of basalt at 1,430 K is approximately zero, especially in the anorthite–diopside, anorthite–diopside–forsterite, and forsterite–diopside–SiO_2 systems. With this assumption, the enthalpy of melting of basalt is:

$$\Delta H_f(T)_{\mathrm{basalt}} = \sum n_i H_i(T) + \Delta H_{\mathrm{m}}(T) \qquad (11)$$

where n_i is the number of moles of endmember i and ΔH_{m} is the enthalpy of mixing at temperature T of the major end-members of basalt (Navrotsky et al. 1989; Tarina et al. 1994; Navrotsky 1995; Brown and Navrotsky 1994). The various $H_i(T)$ of the major end-members of basalt used in Eq. 12 are reported in Table 6 for two temperatures T_{f} and $T = 1{,}430$ K.

Lange et al. (1994) determined enthalpy profiles during melting and crystallization of an olivine basalt as a function of cooling and heating rates. For comparison purposes, we have determined by differential thermal analysis the enthalpy profile during melting for SFB basalt heated at a rate of 10 K/min. The results indicate that the heat effect is resolved over an interval of about 270 K for the SFB sample (Fig. 7). This interval is wider than obtained by Lange et al. (1994) for an olivine basalt heated at a slower rate than in our experiments. This confirms the observation made by Lange et al. (1994) that the temperature interval over which a heat effect can be resolved widens with increasing heating rate, at least for heating rates ranging from 1 to 10 K/min.

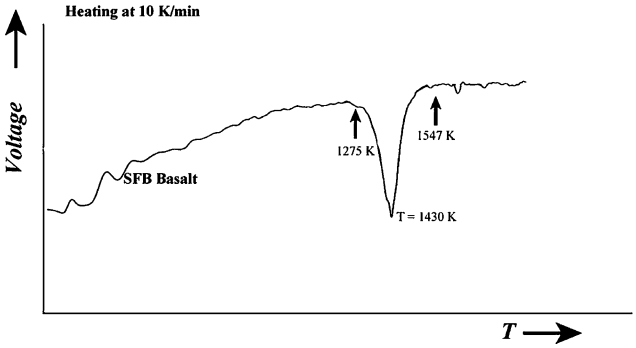

Fig. 7 Typical endothermic peak during melting observed in differential scanning calorimetry (at 10 K/min) for SFB basalt. Also shown are the liquidus and the temperature interval of the heat effect

Table 6 Enthalpies of melting ΔH_{f} (kJ/mol) at T_{f} and 1,430K

Composition	T_{f} (K)	ΔH_{f} (T_{f})	ΔH_{f} (1430 K)
$NaAlSi_3O_8$	1,393	64.5	64.8
$KAlSi_3O_8$	1,500	54.0	53.6
$CaAl_2Si_2O_8$	1,830	133.0	123.7
$CaMgSi_2O_6$	1,670	82.5	78.4
Mg_2SiO_4	2,174	142.0	128.3
Fe_2SiO_4	1,490	89.3	88.8
$FeTiO_3$	1,640	21.7	17.9

From the data of Richet and Bottinga (1984a, b) and Richet et al. (1993b), Stebbins and Carmichael (1984) and Naylor and Cook (1946)

Conclusions

The heat capacities of the glassy and crystalline phases can be predicted to within ±2% with the models of Richet (1987) and Berman and Brown (1985), respectively. A similar precise prediction of heat capacities for the crystalline phase can be obtained by considering the heat capacities of the constituent minerals of basalt.

For the liquid phase the heat capacity of basalt can be reproduced by a constant value (1.5223 J/g K) within a wide range of temperature (from 960 to 1,800 K). This constant value is in good agreement with the models of Stebbins et al. (1984) and Lange and Navrotsky (1992) (within 0.7 and 0.3%, respectively). Using the heat capacities of the molten minerals, however, one can reproduce measured values to within 2%.

Calculation of the enthalpy of fusion of the basalt from the heat capacities of the three phases and the enthalpy of vitrification, yields values of about 400 J/g at 1430 K and 506 J/g at 1530 K. This result is in good agreement with the most recent experimental data, and suggest a near-zero value for the enthalpy of mixing between the different constituent minerals of the basalt composition.

Finally, the enthalpy of formation at 298 K from the oxides of the crystalline and glass phases of Stein-Frentz basalt are readily calculated from the enthalpies of formation listed by Robie et al. (1979) for individual minerals, the observed mineralogical composition and the enthalpy of vitrification determined in this paper. The results are –112.2 and –98.5 kJ/mol, respectively.

Acknowledgments We thank C. Téqui for help with the drop-calorimetry measurements; A. Whittington for helpful comments; and R. Lange and an anonymous reviewer for thoughtful reviews of this paper. This work has benefited from the EU project ENV4-CT98-0713 « Parametrisation and Modelling of Lava Flows ». In addition, MAB and AN gratefully acknowledge support by the grants NERC No. NER/A/S/2003/00378 and EAR 0229332, respectively.

References

Asimow PD, Hirschmann MM, Stolper EM (2001) Calculation of peridodite partial melting from thermodynamic models of minerals and melts, IV. Adiabatic decompression and the composition and mean properties of Mid-Ocean Ridge Basalts. J Petrol 42:963–998

Bacon CR (1977) High-temperature heat content and heat capacity of silicate glasses: experimental determination and model for calculation. Am J Sci 277:109–135

Barus C (1893) The fusion constants of igneous rock. III. The thermal capacity of igneous rock, considered in its bearing on the relation of melting-point to pressure. Phil Mag 35:296–307

Berman RG, Brown TH (1985) Heat capacity of minerals in the system Na_2O–K_2O–CaO–MgO–FeO–Fe_2O_3–Al_2O_3–SiO_2–TiO_2–H_2O–CO_2: representation, estimation and high-temperature extrapolation. Contrib Mineral Petrol 89:168–183

Bouhifd MA, Courtial P, Richet P (1998) Configurational heat capacities: alkali vs. alkaline–earth aluminosilicate liquids. J Noncrystal Solids 231:169–177

Bouhifd MA, Richet P, Besson P, Roskosz M, Ingrin J (2004) Redox state, microstructure and viscosity of a partially crystallized basalt melt. Earth Planet Sci Lett 218:31–44

Bowen NL (1913) The melting phenomena of plagioclase feldspars, Am J Sci 35:577–599

Brown NE, Navrotsky A (1994) Hematite–ilmenite (Fe_2O_3–$FeTiO_3$) solid solutions: the effects of cation ordering on the thermodynamics of mixing. Am Mineral 79:485–496

Burchfield JD (1990) Lord Kelvin and the age of the Earth. 2nd edn. The University of Chicago Press, Chicago

Courtial P, Richet P (1993) Heat capacity of magnesium aluminosilicate melts. Geochim Cosmochim Acta 57:1267–1275

DeYoreo JJ, Lange RA, Navrotsky A (1995) Scanning calorimetric determinations of the heat contents of diopside-rich systems during melting and crystallization. Geochim Cosmochim Acta 59:2701–2707

Fukuyama H (1985) Heat of fusion of basaltic magma. Earth Planet Sci Lett 73:407–414

Ghiorso MS, Sack RO (1995) Chemical mass transfer in magmatic processes IV. A revised and internally consistent thermodynamic model for the interpolation and extrapolation of liquid–solid equilibria in magmatic systems at elevated temperatures and pressures. Contrib Mineral Petrol 119:197–212

Gillet P, Richet P, Guyot F, Fiquet G (1991) High-temperature thermodynamic properties of forsterite. J Geophy Res 96:11805–11816

Holland TJB, Powell R (1998) An internally consistent thermodynamic data set for phases of petrological interest. J Metamorphic Geol 16:309–343

King C (1893) The age of the Earth. Am J Sci 45:1–20

Kilinc A, Carmichael ISE, Rivers ML, Sack RO (1983) The ferric–ferrous ratio of natural silicate liquids equilibrated in air. Contrib Mineral Petrol 83:136–140

Kojitani H, Akaogi M (1995) Measurement of heat of fusion of model basalt in the system diopside–forsterite–anorthite. Geophys Res Lett 22:2329–2332

Kojitani H, Akaogi M (1997) Melting enthalpies of mantle peridotite: calorimetric determinations in the system CaO–MgO–Al_2O_3–SiO_2 and application to magma generation. Earth Planet Sci Lett 153:209–222

Kress VC, Carmichael ISE (1988) Stoichiometry of the iron oxidation reaction in silicate melts. Am Mineral 73:1267–1274

Lange RA, Navrotsky A (1992) Heat capacities of Fe_2O_3-bearing silicate liquids. Contrib Mineral Petrol 110:311–320

Lange RA, DeYoreo JJ, Navrotsky A (1991) Scanning calorimetry measurement of heat capacity during incongruent melting of diopside. Am Mineral 76:904–912

Lange RA, Cashman KV, Navrotsky A (1994) Direct measurements of latent heat during crystallization and melting of a ugandite and an olivine basalt. Contrib Mineral Petrol 118:169–181

Lindroth DP, Krawza WG (1971) Heat content and specific heat of six rock types at temperatures to 1000°C. Rept Inv, 7503, US Bureau of Mines, Washington, 24 pp

Navrotsky A (1995) Energetics of silicate melts. In: Stebbins JF, McMillan PF, Dingwell DB (eds) Structure, dynamics and properties of silicate melts. Rev Mineral 32:121–143

Navrotsky A (1997) Progress and new directions in high-temperature calorimetry revisited. Phys Chem Mineral 24:222–241

Navrotsky A, Ziegler D, Oestrike R, Maniar P (1989) Calorimetry of silicate melts at 1773 K: measurements of the enthalpies of fusion and of mixing in the systems diopside–anorthite–albite and anorthite–forsterite. Contrib Mineral Petrol 101:122–130

Naylor BF, Cook OA (1946) High-temperature heat contents of the metatitanates of calcium, iron and magnesium. J Am Chem Soc 68:1003–1005

Osborn EF, Tait DB (1952) The system diopside–forsterite–anorthite. Am J Sci Bowen ***vol, pp 413–433

Richet P (1987) Heat capacity of silicate glasses. Chem Geol 62:111–124

Richet P, Bottinga Y (1984a) Anorthite, andesine, diopside, wollastonite, cordierite and pyrope: thermodynamics of melting, glass transitions, and properties of the amorphous phases. Earth Planet Sci Lett 67:415–432

Richet P, Bottinga Y (1984b) Glass transitions and thermodynamic properties of $NaAlSinO_{2n+2}$ and $KalSi_3O_8$. Geochim Cosmochim Acta 48:453–470

Richet P, Bottinga Y (1985) Heat capacity of aluminium-free liquid silicates. Geochim Cosmochim Acta 49:471–486

Richet P, Bottinga Y (1986) Thermochemical properties of silicate glasses and liquids: a review. Rev Geophys 24:1–25

Richet P, Bottinga Y, Denielou L, Petitet JP, Téqui C (1982) Thermodynamic properties of quartz, cristobalite and amorphous SiO_2: drop calorimetry measurements between 1000 and 1800 K and a review from 0 to 2000 K. Geochim Cosmochim Acta 46:2639–2658

Richet P, Gillet P, Fiquet G (1992) Thermodynamic properties of minerals: macroscopic and microscopic approaches. In: Saxena SK (ed) Adv Phys Geochem Springer, Heidelberg 10:98–131

Richet P, Fiquet G (1991) High-temperature heat capacity and premelting of minerals in the system CaO–MgO–Al_2O_3–SiO_2. J Geophys Res 96:445–456

Richet P, Leclerc F, Benoist L (1993a) Melting of forsterite and spinel, with implications for the glass transition of Mg_2SiO_4 liquid. Geophys Res Lett 20:1675–1678

Richet P, Robie RA, Hemingway BS (1993b) Entropy and structure of silicate glasses and melts. Geochim Cosmochim Acta 57:2751–2766

Roberts-Austen WC, Rücker AW (1891) On the specific heat of basalt. Phil Mag 32:353–355

Robie RA, Hemingway BS, Fisher JR (1979) Thermodynamic properties of minerals and related substances at 298.15 K and 1 bar (10^5 pascals) pressure and at higher temperatures. US Geol Surv Bull vol 1452, 456 p

Robie RA, Hemingway BS (1995) Thermodynamic properties of minerals and related substances at 298.15 K and 1 bar (10^5 Pascals) pressure and at higher temperatures. US Geol Surv Bull, vol 2131, 461 pp

Robinson GR, Haas JL (1983) Heat capacity, relative enthalpy, and calorimetric entropy of silicate minerals: an empirical method of prediction. Am Mineral 68:541–553

Stebbins JF, Carmichael ISE, Weill DF (1983) The high temperature liquid and glass heat contents and the heats of fusion of diopside, albite, sanidine and nepheline. Am Mineral 68:717–730

Stebbins JF, Carmichael ISE (1984) The heat of fusion of fayalite. Am Mineral 69:292–297

Stebbins JF, Carmichael ISE, Moret LK (1984) Heat capacities and entropies of silicate liquids and glasses. Contrib Mineral Petrol 86:131–148

Sugawara T, Akaogi M (2003) Heats of mixing of silicate liquid in the systems diopside–anorthite–akermanite, diopside–anorthite–forsterite, and diopside–silica. Am Mineral 88:1020–1024

Tarina I, Navrotsky A, Gan H (1994) Direct calorimetric measurement of enthalpies in diopside–anorthite–wollastonite melts at 1773 K. Geochim Cosmochim Acta 58:3665–3673

Tsuruta K, Takahashi E (1998) Melting study of an alkali basalt JB-1 up to 12.5 GPa: behavior of potassium in the deep mantle. Phys Earth Planet Interiors 107:119–130

Weill DF, Stebbins JF, Hon R, Carmichael ISE (1980) The enthalpy of fusion of anorthite. Contrib Mineral Petrol 74:95–102

Yoder HS (1976) Generation of basaltic magma. National Academy of Sciences, Washington, 246 pp

Yoder HS, Tilley CE (1962) Origin of basalt magmas: an experimental study of natural and synthetic rock systems. J Petrol 3:342–532

Ziegler D, Navrotsky A (1986) Direct measurement of the enthalpy of fusion of diopside. Geochim Cosmochim Acta 50:2461–2466